

## Fluorescent Probes

## Investigating Intracellular Localisation and Cytotoxicity Trends for Neutral and Cationic Iridium Tetrazolato Complexes in Live Cells

Chiara Caporale,<sup>[a]</sup> Christie A. Bader,<sup>[b]</sup> Alexandra Sorvina,<sup>[b]</sup> Karen D. M. MaGee,<sup>[a]</sup> Brian W. Skelton,<sup>[c]</sup> Todd A. Gillam,<sup>[b]</sup> Phillip J. Wright,<sup>[a]</sup> Paolo Raiteri,<sup>[d]</sup> Stefano Stagni,<sup>[e]</sup> Janna L. Morrison,<sup>[g]</sup> Sally E. Plush,<sup>\*,[b, f]</sup> Douglas A. Brooks,<sup>\*,[b]</sup> and Massimiliano Massi<sup>\*,[a]</sup>

**Abstract:** A family of five neutral cyclometalated iridium(III) tetrazolato complexes and their methylated cationic analogues have been synthesised and characterised. The complexes are distinguished by variations of the substituents or degree of  $\pi$  conjugation on either the phenylpyridine or tetrazolato ligands. The photophysical properties of these species have been evaluated in organic and aqueous media, revealing predominantly a solvatochromic emission originating from mixed metal-to-ligand and ligand-to-ligand charge transfer excited states of triplet multiplicity. These emissions are characterised by typically long excited-state lifetimes (~hundreds of ns), and quantum yields around 5–10% in

aqueous media. Methylation of the complexes caused a systematic red-shift of the emission profiles. The behaviour and the effects of the different complexes were then examined in cells. The neutral species localised mostly in the endoplasmic reticulum and lipid droplets, whereas the majority of the cationic complexes localised in the mitochondria. The amount of complexes found within cells does not depend on lipophilicity, which potentially suggests diverse uptake mechanisms. Methylated analogues were found to be more cytotoxic compared to the neutral species, a behaviour that might be linked to a combination of uptake and intracellular localisation.

[a] C. Caporale, K. D. M. MaGee, Dr. P. J. Wright, Prof. M. Massi  
Curtin Institute of Functional Molecules and Interfaces and  
Department of Chemistry, Curtin University,  
Kent Street, Bentley 6102 WA (Australia)  
E-mail: m.massi@curtin.edu.au

[b] Dr. C. A. Bader, Dr. A. Sorvina, T. A. Gillam, Dr. S. E. Plush, Prof. D. A. Brooks  
Mechanisms in Cell Biology and Disease Research Group,  
School of Pharmacy and Medical Sciences,  
Sansom Institute for Health Research,  
University of South Australia, Adelaide (Australia)  
E-mail: sally.plush@unisa.edu.au  
doug.brooks@unisa.edu.au

[c] Prof. B. W. Skelton  
School of Molecular Sciences, University of Western Australia,  
35 Stirling Highway, Crawley, Perth, WA 6009 (Australia)

[d] Prof. P. Raiteri  
Curtin Institute for Computation and Department of Chemistry,  
Curtin University, Kent Street, Bentley 6102 WA (Australia)

[e] Prof. S. Stagni  
Department of Industrial Chemistry "Toso Montanari"-  
University of Bologna, viale del Risorgimento 4, Bologna 40136 (Italy)

[f] Dr. S. E. Plush  
Future Industries Institute, University of South Australia,  
Mawson Lakes, SA 5095 (Australia)

[g] Prof. J. L. Morrison  
Early Origins of Adult Health Research Group,  
School of Pharmacy and Medical Sciences,  
Sansom Institute for Health Research,  
University of South Australia, Adelaide, South Australia 5000 (Australia)

Supporting information and the ORCID identification number(s) for the author(s) of this article can be found under <https://doi.org/10.1002/chem.201701352>

## Introduction

Luminescent metal complexes of transition [for example, Ru<sup>II</sup>, Re<sup>I</sup>, Ir<sup>III</sup>, Au<sup>I</sup>, and Pt<sup>II</sup>]<sup>[1–4]</sup> and lanthanoid elements [for example, Eu<sup>III</sup> and Tb<sup>III</sup> for visible emission; Yb<sup>III</sup> for near-infrared emission]<sup>[5,6]</sup> have specific photophysical properties that are ideal for cellular imaging. These properties have the potential to solve some of the critical drawbacks associated with more traditionally investigated organic fluorophores.<sup>[7]</sup> Appropriately designed metal complexes exhibit enhanced photostability, and therefore do not suffer from rapid photobleaching, allowing for imaging at longer time scales.<sup>[1]</sup> Luminescent heavy-metal complexes are also typically characterised by large Stokes shifts, which prevents concentration quenching phenomena.<sup>[1]</sup> Furthermore, their relatively longer excited-state lifetimes make this class of luminophores amenable to time-gated imaging to improve signal-to-noise ratio by minimising interference from fast-decaying autofluorescence.<sup>[8]</sup>

Luminescent cyclometalated iridium(III) complexes are proving to be exceptional systems for the development of markers for live cell imaging.<sup>[9,10]</sup> The chemical, photophysical, and biological targeting properties of these complexes can be readily varied by altering the coordinating ligands or by chemical coupling.<sup>[11,12]</sup> In addition, their absorption and emission profiles can be modulated along the spectral range of visible light from blue to red, and further into the near-infrared region, by introducing appropriate functional groups or by the variation of the  $\pi$  conjugation on the aromatic ligands.<sup>[13,14]</sup> Following similar principles, the lipophilicity of these complexes can be

adjusted to favour transport across the cellular membrane, while maintaining adequate solubility in aqueous media.<sup>[1,15]</sup> A large number of luminescent iridium complexes have been reported to possess not only the capacity to internalise into cells,<sup>[13,16]</sup> but also the ability to accumulate within specific organelles such as mitochondria,<sup>[17–22]</sup> lysosomes,<sup>[15,23–25]</sup> nuclei,<sup>[26–30]</sup> and endoplasmic reticulum.<sup>[31–34]</sup> Some iridium complexes have been conjugated with biologically relevant moieties such as carbohydrates,<sup>[18,35]</sup> biotin/avidin,<sup>[36–39]</sup> amino acids,<sup>[23]</sup> and proteins,<sup>[40]</sup> in an attempt to impart and control their biospecificity. Furthermore, examples of complexes with the ability to sense targeted biological species via reversible or irreversible modulation of their photophysical properties have also been reported.<sup>[21,27,34,41–47]</sup>

A rationalisation of the structure–activity relationship (SAR) of luminescent iridium complexes is still difficult to achieve from the current knowledge base. This is partly due to the fact that labelling experiments are often carried out with a diverse range of complexes using different cell lines or model systems. Moreover, the staining protocols used are often variable when comparing data from different research groups.<sup>[48]</sup> In addition, a priority has been given to producing cationic iridium complexes, seemingly arising from the fact that they might possess increased solubility in aqueous media and exhibit more favourable membrane transport by exploiting membrane potential gradients. However, many of these molecular complexes have exhibited moderate to acute cytotoxicity, a property that can be regarded favourably for the joint development of therapeutics,<sup>[22,24,49–51]</sup> but which is not ideal for visualising cellular functions in live cell systems. Notably, only a handful of neutral iridium complexes have been investigated as cellular imaging agents.<sup>[15,23,25,47,52,53]</sup>

We previously showed that neutral luminescent rhenium(I) complexes can be used for live cell imaging, offering different

biospecificity to the more popularly investigated cationic rhenium complexes.<sup>[54]</sup> For example, we demonstrated unprecedented staining of polar lipids in live cells using the complex *fac*-[Re(CO)<sub>3</sub>(phen)L] (L = 5-(4-cyanophenyl)tetrazolate; phen = 1,10-phenanthroline).<sup>[55,56]</sup> Furthermore, simple chemical modulation of the tetrazolato ancillary ligand has been a viable strategy to impart alternative biological behaviour, with successful staining of the endoplasmic reticulum and the visualisation of membrane events in live cells.<sup>[57]</sup> We have now focused our attention on the investigation of cyclometalated iridium complexes bound to tetrazolato ligands, which is a family of neutral and analogous cationic iridium species that have not been previously used as molecular probes for live cell imaging. For this scope, we prepared an initial library of complexes by modifying the functional groups on the ligands and by the extension of the  $\pi$  conjugation (Figure 1). Due to the intrinsic reactivity of the coordinated tetrazolato ligand towards electrophiles,<sup>[11,58,59]</sup> these neutral complexes could also be easily methylated to form the analogous cationic species. This approach allowed the preparation of a family of complexes for a more systematic SAR investigation that can relate how variations in the chemical structure and charge might influence the biological behaviour of the iridium markers in relation to cellular incubation, localisation, and cytotoxicity.

## Results and Discussion

### Synthesis of the tetrazolato ligands and corresponding iridium complexes

The adopted synthetic procedures are shown in Figure 2. The ligand precursor 2,5-dicyanopyridine was obtained in three steps starting from commercially available 2,5-pyridinedicarboxylic acid. Following a Fisher esterification to form the

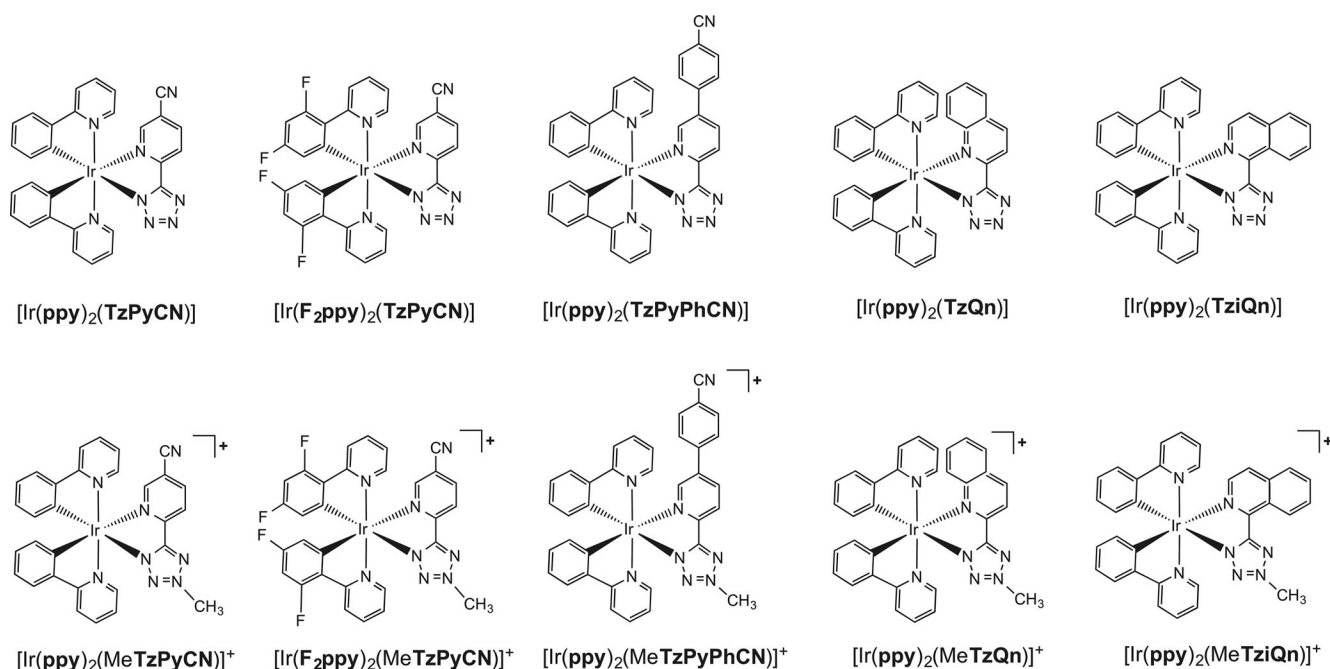


Figure 1. Neutral and cationic iridium tetrazolato complexes synthesised and investigated for live cell imaging.

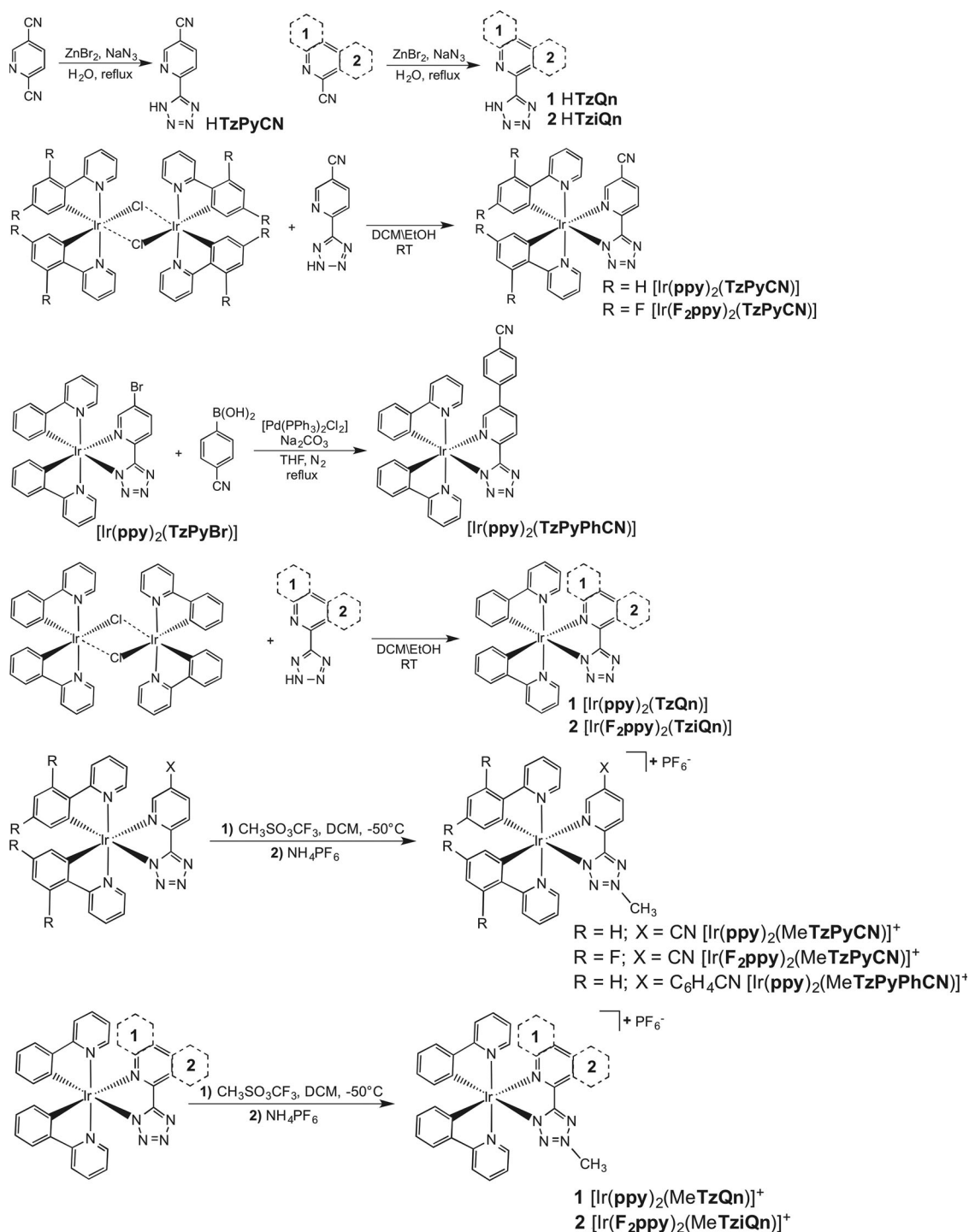


Figure 2. Summary of the synthetic procedures for the preparation of the iridium complexes.

corresponding methyl ester groups, aminolysis with aqueous ammonia gave the corresponding primary amides. Lastly, dehydration of the amide groups yielded the desired nitrile moieties.<sup>[60]</sup> Following a methodology developed by Sharpless,<sup>[61]</sup> 2,5-dicyanopyridine was reacted with sodium azide in the presence of zinc bromide in water at reflux, yielding the HTzPyCN ligand. Complete separation of HTzPyCN from the ditetrazole byproduct (present in 5–10% molar amount determined by NMR analysis) by selective protonation was challenging, and

the impure HTzPyCN was used as recovered for complexation with iridium. The ligands HTzQn and HTziQn were synthesised following the same methodology.

To prepare the family of neutral iridium complexes [Ir(ppy)<sub>2</sub>(TzPyCN)], [Ir(F<sub>2</sub>ppy)<sub>2</sub>(TzPyCN)], [Ir(ppy)<sub>2</sub>(TzQn)], and [Ir(ppy)<sub>2</sub>(TziQn)], the corresponding chloro-bridged iridium dimers (bearing either ppy or F<sub>2</sub>ppy as cyclometalating ligands) were reacted with a slight excess of the corresponding pyridyl or (iso)quinolyl tetrazolato species.<sup>[11]</sup> The complex

[Ir(ppy)<sub>2</sub>(TzPyPhCN)] was prepared via a different route, involving a Suzuki coupling of the previously reported [Ir(ppy)<sub>2</sub>(TzPyBr)]<sup>[11]</sup> with 4-cyanophenylboronic acid. Previous attempts to react the iridium chloro-bridged dimer with the preformed corresponding tetrazolato ligand were unsuccessful, as an inseparable mixture of products was obtained. Methylation of all the neutral complexes was performed by treatment with methyl trifluoromethanesulphonate, followed by metathesis with ammonium hexafluorophosphate.<sup>[11]</sup> All the synthesised complexes were characterised by means of NMR (see the Supporting Information for all the <sup>1</sup>H and <sup>13</sup>C NMR spectra) and IR spectroscopy as well as elemental analysis.

### X-ray structural determination

Single crystals suitable for X-ray diffraction were obtained for the neutral [Ir(F<sub>2</sub>ppy)<sub>2</sub>(TzPyCN)] and the charged [Ir(ppy)<sub>2</sub>(MeTzPyPhCN)]<sup>+</sup>[PF<sub>6</sub><sup>-</sup>] complexes. These species crystallized in the monoclinic *I2/a* and *P2/n* space groups, respectively (Figure 3). The coordination arrangement of the ligands is

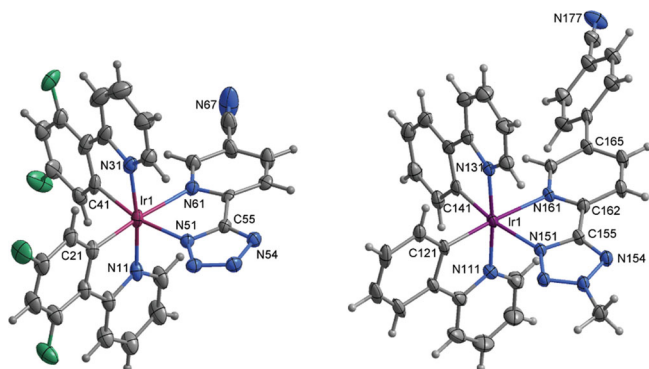


**Figure 3.** X-ray crystal structures of [Ir(F<sub>2</sub>ppy)<sub>2</sub>(TzPyCN)] (left) and [Ir(ppy)<sub>2</sub>(MeTzPyPhCN)]<sup>+</sup> (right), with displacement ellipsoids drawn at the 50% probability level. Lattice solvent molecules and counter anion (PF<sub>6</sub><sup>-</sup>) are omitted for clarity.

analogous, with the two pyridine rings of the phenylpyridine ligands adopting a *trans* configuration, whereas the two cyclometalated phenyl rings are arranged in *cis* configuration. The rest of the coordination sphere is occupied by the two nitrogen atoms of the tetrazole and pyridine rings. The [Ir(ppy)<sub>2</sub>(MeTzPyPhCN)]<sup>+</sup>[PF<sub>6</sub><sup>-</sup>] complex highlights methylation of the tetrazole ring at the N3 position.

### Photophysical properties

A summary of the photophysical properties for the synthesised iridium complexes, measured from dichloromethane and aqueous (ca. 10<sup>-5</sup> M) solutions are listed in Table 1 (see the Supporting Information for photophysical data in PBS, lysosomal pH fluid solution, and ethyl laurate). The aqueous media contained about 0.2% DMSO to favour the solubilisation of the iridium complexes. The various solvents have been chosen to identify potential modulations of the photophysical properties of the

iridium complexes in diverse cellular environments such as cytoplasm, endosomes, acidic organelles (e.g. lysosomes), and lipid-rich compartments like membranes, endoplasmic reticulum, and lipid droplets. The photophysical properties were measured in air-equilibrated solutions to account for the presence of oxygen in live cells. However, to confirm triplet multiplicity of the excited states, the measurements were also performed in degassed dichloromethane solutions.<sup>[62]</sup>

The absorption spectra from air-equilibrated dichloromethane solutions are presented in Figure 4 (for the spectral profiles in other solvents see the Supporting Information). All the

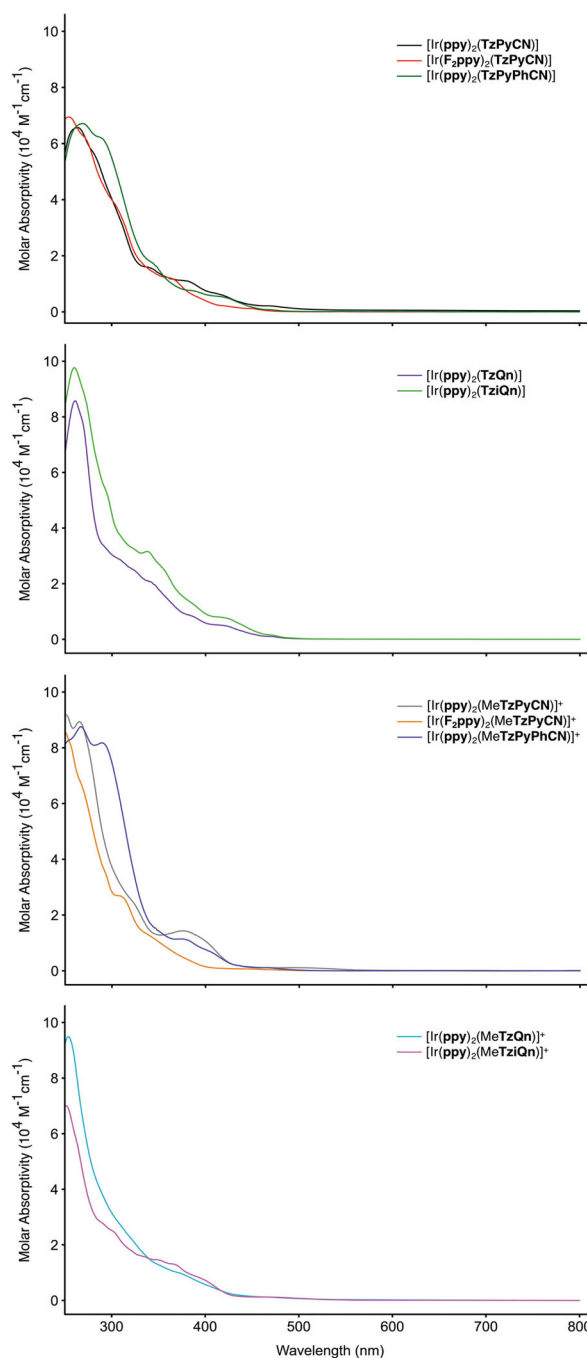


**Figure 4.** Absorption spectra of the iridium complexes from 10<sup>-5</sup> M air-equilibrated dichloromethane solutions.

**Table 1.** Photophysical data of the iridium complexes from  $10^{-5}$  M dichloromethane and aqueous solutions.

Complex	Solvent <sup>[a]</sup>	$\lambda_{\text{abs}}$ [nm] ( $10^3 \epsilon$ [ $\text{M}^{-1} \text{cm}^{-1}$ ])	$\lambda_{\text{em}}$ [nm]	$\tau_{\text{aer}}$	$\Phi_{\text{aer}}$
				$\tau_{\text{deaer}}$ [ns] <sup>[b]</sup>	$\Phi_{\text{deaer}}$ <sup>[c]</sup>
[Ir(ppy) <sub>2</sub> (TzPyCN)]	CH <sub>2</sub> Cl <sub>2</sub>	263 (6.57), 339 (1.59), 382 (1.09), 420 (0.58)	618	131 529	0.055 0.397
	H <sub>2</sub> O	253 (3.52), 377 (0.69)	618	123 (25), 440 (75) _ [d]	0.047 _ [d]
[Ir(F <sub>2</sub> ppy) <sub>2</sub> (TzPyCN)]	CH <sub>2</sub> Cl <sub>2</sub>	256 (5.20), 364 (0.95)	542	140 697	0.042 0.406
	H <sub>2</sub> O	256 (4.83), 302 (3.36), 366 (1.16)	552	189 (41), 628 (59) _ [d]	0.057 _ [d]
[Ir(ppy) <sub>2</sub> (TzPyPhCN)]	CH <sub>2</sub> Cl <sub>2</sub>	268 (3.95), 290 (3.64), 345 (0.58), 423 (0.27)	560	114 880	0.023 0.149
	H <sub>2</sub> O	286 (1.87), 350 (0.86), 421 (0.34)	580	200 (31), 728 (69) _ [d]	0.055 _ [d]
[Ir(ppy) <sub>2</sub> (MeTzPyCN)] <sup>+</sup>	CH <sub>2</sub> Cl <sub>2</sub>	266 (8.93), 376 (1.44)	680	31 (79), 168 (21) 35 (61), 362 (39) _ [e]	0.012 0.014 _ [e]
	H <sub>2</sub> O	260 (4.44), 373 (0.59)	_ [e]	_ [e]	_ [e]
[Ir(F <sub>2</sub> ppy) <sub>2</sub> (MeTzPyCN)] <sup>+</sup>	CH <sub>2</sub> Cl <sub>2</sub>	250 (3.56), 316 (1.28), 356 (0.58)	600	287 551	0.057 0.188
	H <sub>2</sub> O	260 (4.12), 309 (1.55), 353 (0.66)	636	11 (76), 56 (24) _ [d]	0.005 _ [d]
[Ir(ppy) <sub>2</sub> (MeTzPyPhCN)] <sup>+</sup>	CH <sub>2</sub> Cl <sub>2</sub>	267 (3.39), 290 (3.14), 378 (0.40)	600	184 434	0.057 0.093
	H <sub>2</sub> O	264 (3.82), 390 (0.35)	605	17 (22), 320 (88) _ [d]	0.005 _ [d]
[Ir(ppy) <sub>2</sub> (TzQn)]	CH <sub>2</sub> Cl <sub>2</sub>	263 (8.44), 345 (1.97), 428 (0.42)	580	153 831	0.021 0.065
	H <sub>2</sub> O	266 (4.41), 350 (2.35), 425 (0.97)	600	305 (25), 928 (75) _ [d]	0.039 _ [d]
[Ir(ppy) <sub>2</sub> (TziQn)]	CH <sub>2</sub> Cl <sub>2</sub>	260 (9.77), 340 (3.13), 424 (0.75)	575	497 6713	0.036 0.144
	H <sub>2</sub> O	268 (3.42), 350 (2.00), 435 (0.80)	590	217 (33), 531 (67) _ [d]	0.018 _ [d]
[Ir(ppy) <sub>2</sub> (MeTzQn)] <sup>+</sup>	CH <sub>2</sub> Cl <sub>2</sub>	257 (9.29), 376 (0.95)	635	218 546	0.028 0.043
	H <sub>2</sub> O	251 (8.30), 307 (2.52), 364 (1.09)	630	17 (39), 134 (61) _ [d]	0.004 _ [d]
[Ir(ppy) <sub>2</sub> (MeTziQn)] <sup>+</sup>	CH <sub>2</sub> Cl <sub>2</sub>	253 (6.96), 303 (2.45), 371 (1.24)	640	208 485	0.049 0.063
	H <sub>2</sub> O	251 (6.64), 291 (2.60), 355 (1.36)	660	9 (53), 93 (47) _ [d]	0.004 _ [d]

[a] Aqueous solutions contain 0.2% DMSO. [b] For the biexponential excited state lifetime ( $\tau$ ), the relative weights of the exponential curves are reported in parentheses;  $\tau_{\text{deaer}}$  is reported only for dichloromethane solutions. [c] Measured versus [Ru(bpy)<sub>3</sub>]<sup>2+</sup> in H<sub>2</sub>O ( $\Phi_r = 0.028$ ). [d] Measurements in aqueous solutions were only performed in air-equilibrated conditions. [e] Not emissive.

iridium complexes show intense absorption bands in the UV region (250–300 nm), which are associated with ligand-centred (LC)  $\pi-\pi^*$  transitions, followed by bands of lower intensity tailing off into the visible region of the spectra. These lower energy bands are ascribed to spin allowed (singlet to singlet) and spin forbidden (singlet to triplet) ligand-to-ligand (LLCT) and metal-to-ligand charge transfer (MLCT) transitions.<sup>[11]</sup>

Excitation of the iridium complexes at 375 nm results in long-lived orange to red emission in air-equilibrated dichloromethane solutions, and the emission spectra measured at 298 K are shown in Figure 5 (for the emission spectra in other solvents see SI). The neutral complexes [Ir(ppy)<sub>2</sub>(TzPyCN)], [Ir(F<sub>2</sub>ppy)<sub>2</sub>(TzPyCN)], and [Ir(ppy)<sub>2</sub>(TzPyPhCN)] are characterised by broad and featureless emission bands, that are typical for radiative decays from excited states of charge transfer

character.<sup>[12]</sup> The [Ir(ppy)<sub>2</sub>(TzPyCN)] complex presents a red-shifted maximum at 618 nm, which is ascribed to a stabilisation of the unoccupied  $\pi^*$  orbitals localised on the TzPyCN<sup>-</sup> ligand caused by the electron-withdrawing nature of the nitrile functional group.<sup>[11]</sup> As expected, the addition of electron-withdrawing fluoride substituents on the ppy ligands causes a blue-shift of the emission maximum for [Ir(F<sub>2</sub>ppy)<sub>2</sub>(TzPyCN)] ( $\lambda_{\text{em}} = 542$  nm), as a consequence of the stabilisation of the occupied  $\pi$  orbitals of the ligands and iridium 5d orbitals composing the mixed LLCT(F<sub>2</sub>ppy → TzPyCN) and MLCT(Ir → TzPyCN) transition.<sup>[11]</sup> The emission maximum of [Ir(ppy)<sub>2</sub>(TzPyPhCN)] at 560 nm is again blue-shifted with respect to [Ir(ppy)<sub>2</sub>(TzPyCN)], albeit to a lesser extent when compared to [Ir(F<sub>2</sub>ppy)<sub>2</sub>(TzPyCN)]. This trend is ascribed to the fact that the electron-withdrawing effect of the nitrile group on the

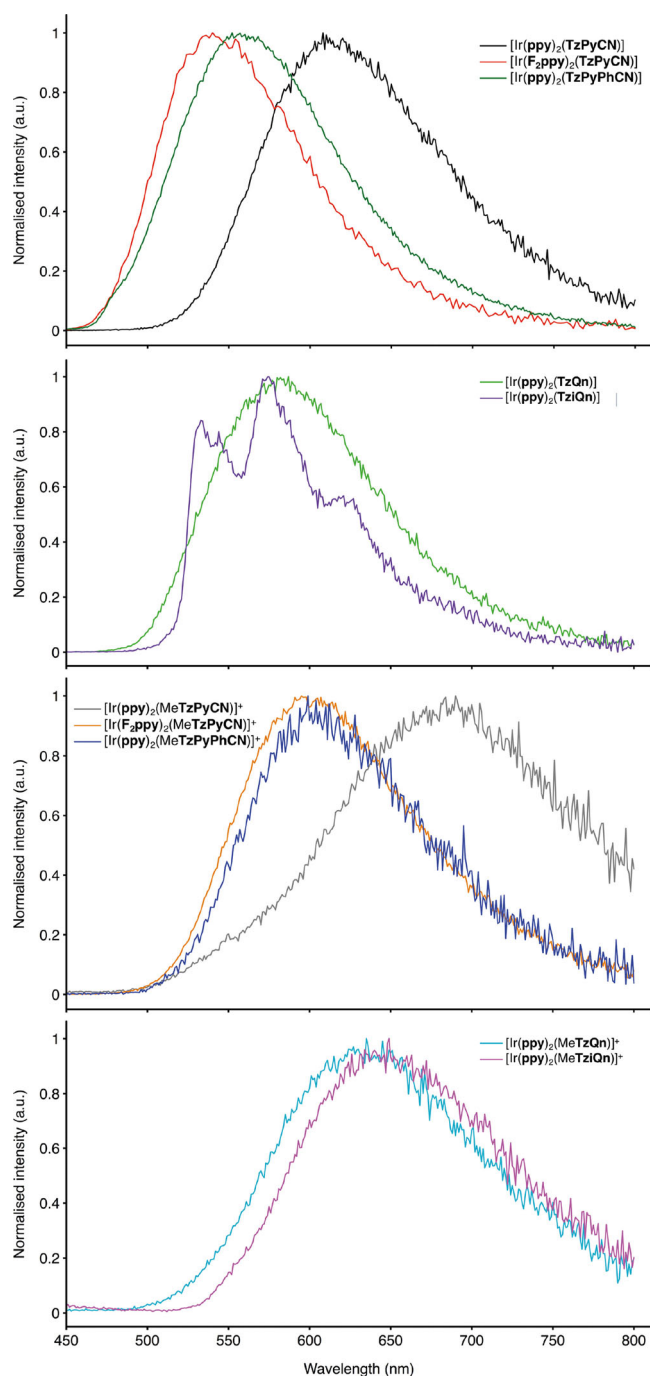


**Figure 5.** Emission spectra of the iridium complexes from approximately  $10^{-5}$  M air-equilibrated dichloromethane solutions with excitation at 375 nm.

pyridyltetrazole  $\pi^*$  system is decreased by the addition of a phenyl ring spacer. The emission profiles of the methylated complexes  $[\text{Ir}(\text{ppy})_2(\text{MeTzPyCN})]^+$  ( $\lambda_{\text{em}} = 680$  nm),  $[\text{Ir}(\text{F}_2\text{ppy})_2(\text{MeTzPyCN})]^+$  ( $\lambda_{\text{em}} = 600$  nm), and  $[\text{Ir}(\text{ppy})_2(\text{MeTzPyPhCN})]^+$  ( $\lambda_{\text{em}} = 600$  nm) are red-shifted compared to their corresponding neutral complexes. Once more, this red-shift demonstrates that the  $\pi^*$  system of the pyridyl tetrazole ligand acts as an electron acceptor in the charge transfer transitions.<sup>[11,63]</sup> When comparing the emission maxima of these three methylated iridium complexes, the trend for the

emission properties is analogous to that observed for their neutral counterparts, with the most red-shifted emission originating from  $[\text{Ir}(\text{ppy})_2(\text{MeTzPyCN})]^+$ .

The iridium complexes containing quinoline and isoquinoline-functionalised tetrazolato ligands,  $[\text{Ir}(\text{ppy})_2(\text{TzQn})]$  and  $[\text{Ir}(\text{ppy})_2(\text{TziQn})]$ , reveal emission bands that are similarly ranging between 500 and 750 nm (Figure 5). Compared to the previously published complex  $[\text{Ir}(\text{ppy})_2(\text{TzPy})]$ ,<sup>[11]</sup> in which  $\text{TzPy}^-$  is 5-(2'-pyridyl)tetrazolate, displaying a structured emission band with peaks at 481 and 510 nm, the complexes  $[\text{Ir}(\text{ppy})_2(\text{TzQn})]$  and  $[\text{Ir}(\text{ppy})_2(\text{TziQn})]$  present a red-shifted emission that is rationalised by the increased  $\pi$  conjugation on passing from a phenyl to a quinolyl or isoquinolyl substituent. The structures of these two bands appear to be quite different. The emission profile of  $[\text{Ir}(\text{ppy})_2(\text{TzQn})]$  is broad and structureless, whereas that of  $[\text{Ir}(\text{ppy})_2(\text{TziQn})]$  appears to be structured with a vibronic progression spaced around  $1300\text{ cm}^{-1}$ . Furthermore, the excited-state lifetime of  $[\text{Ir}(\text{ppy})_2(\text{TziQn})]$  is significantly longer than that of  $[\text{Ir}(\text{ppy})_2(\text{TzQn})]$  (Table 1). These results suggest the presence of a more dominating charge transfer character for the emission of  $[\text{Ir}(\text{ppy})_2(\text{TzQn})]$ .<sup>[64]</sup> On the other hand, the excited state of  $[\text{Ir}(\text{ppy})_2(\text{TziQn})]$  seems to be strongly influenced by LC character.<sup>[64]</sup> To confirm this assumption, we performed time-dependent density functional theory (TD-DFT) analysis on  $[\text{Ir}(\text{ppy})_2(\text{TzQn})]$  and  $[\text{Ir}(\text{ppy})_2(\text{TziQn})]$  (see the Supporting Information). The results show that the lower energy bands are mainly composed of MLCT and LLCT transitions. However, in the case of  $[\text{Ir}(\text{ppy})_2(\text{TziQn})]$ , there is also a contribution from the HOMO-4  $\rightarrow$  LUMO transition corresponding to a LC transition localised on the  $\text{TziQn}^-$  ligand. A further indication of the LC character of the excited state of  $[\text{Ir}(\text{ppy})_2(\text{TziQn})]$  comes from the significantly elongated excited state decay lifetime in degassed dichloromethane, reaching a value of  $6.713\ \mu\text{s}$ .<sup>[65]</sup>

As expected, the emission profiles of the methylated  $[\text{Ir}(\text{ppy})_2(\text{MeTzQn})]^+$  and  $[\text{Ir}(\text{ppy})_2(\text{MeTziQn})]^+$  complexes appear red-shifted, broad, and structureless (Figure 5).

For all the complexes, an elongation of the excited-state lifetime decay ( $\tau$ ) and increase of photoluminescence quantum yield ( $\Phi$ ) values is observed upon degassing. This behaviour is indicative of the triplet spin multiplicity of the excited state.<sup>[12,62]</sup>

The analysis of the emission bands in various solvents reveals solvatochromic behaviour, with a red-shift of the emission maxima upon increasing the polarity of the solvent. The most blue-shifted emission is recorded in ethyl laurate, whereas the emission red-shifts by  $\approx 20\text{--}30$  nm in dichloromethane, with the exception of  $[\text{Ir}(\text{ppy})_2(\text{MeTzPyPhCN})]^+$  and  $[\text{Ir}(\text{ppy})_2(\text{MeTziQn})]^+$  for which almost no shift is observed. The emission bands further shift ( $\approx 10\text{--}30$  nm) towards longer wavelength in aqueous media. There are no significant differences in the various aqueous solvents, apart from  $[\text{Ir}(\text{ppy})_2(\text{MeTzPyPhCN})]^+$  that shows a 22 nm red-shift on passing from PBS to a lysosomal pH fluid solution. The methylated complex  $[\text{Ir}(\text{ppy})_2(\text{MeTzPyCN})]^+$  is found to have appreciable emission only in dichloromethane solution, as the complex is virtually non-emissive in aqueous solvents. In general, the

methylated complexes highlight a greater degree of quenching in aqueous solvents with respect to their neutral analogues. Although conclusive explanations cannot be drawn from these data, potential causes could be ascribed to increased non-radiative decays due to energy gap law and the higher solubility of the cationic complexes in aqueous solvents. In fact, we previously observed a similar behavior for neutral rhenium complexes, in which a decrease of solubility in aqueous media showed an enhanced quantum yield and elongated excited state lifetime.<sup>[54]</sup>

### Lipophilicity

The lipophilicity of the iridium complexes was measured by the shake-flask method using a pH 7.4 buffered PBS solution and *n*-octanol.<sup>[66]</sup> The calculated logD<sub>7.4</sub> values are listed in Table 2. The values obtained are within a range that is similar

**Table 2.** Distribution coefficient values (logD<sub>7.4</sub>) for neutral and methylated iridium complexes.

Complex	logD <sub>7.4</sub>	Molar amount <sup>[a]</sup> [fmol]	Concentration <sup>[b]</sup> [μM]
[Ir(ppy) <sub>2</sub> (TzPyCN)]	2.09 ± 0.06	0.042 ± 0.004	21.16 ± 1.85
[Ir(F <sub>2</sub> ppy) <sub>2</sub> (TzPyCN)]	2.01 ± 0.05	0.319 ± 0.049	159.71 ± 46.95
[Ir(ppy) <sub>2</sub> (TzPyPhCN)]	2.68 ± 0.08	0.171 ± 0.042	85.46 ± 20.76
[Ir(ppy) <sub>2</sub> (MeTzPyCN)] <sup>+</sup>	0.64 ± 0.03	0.015 ± 0.002	7.35 ± 0.81
[Ir(F <sub>2</sub> ppy) <sub>2</sub> (MeTzPyCN)] <sup>+</sup>	1.86 ± 0.02	0.025 ± 0.007	12.74 ± 3.26
[Ir(ppy) <sub>2</sub> (MeTzPyPhCN)] <sup>+</sup>	1.87 ± 0.08	0.045 ± 0.005	22.74 ± 2.48
[Ir(ppy) <sub>2</sub> (TzQn)]	2.23 ± 0.04	0.346 ± 0.070	173.03 ± 35.20
[Ir(ppy) <sub>2</sub> (TziQn)]	2.57 ± 0.05	0.063 ± 0.011	31.61 ± 5.60
[Ir(ppy) <sub>2</sub> (MeTzQn)] <sup>+</sup>	1.68 ± 0.05	0.372 ± 0.038	186.24 ± 18.92
[Ir(ppy) <sub>2</sub> (MeTziQn)] <sup>+</sup>	1.49 ± 0.06	0.515 ± 0.085	257.29 ± 42.64

[a] Average number of moles of iridium complex incubated within a H9c2 cell (see the Experimental Section for incubation conditions). [b] The relative concentration was calculated assuming an average volume of H9c2 cell equal to 2 pL.

to those reported previously for cyclometalated iridium complexes,<sup>[18,24,26,53]</sup> and, in the case of the neutral complexes, fluorophores for the lipid droplets of the BODIPY family (functionalised 4,4-difluoro-4-bora-3a,4a-diaza-s-indacene cores).<sup>[67]</sup> The values for the five neutral complexes are comprised between 2.01 and 2.68. Methylation of the iridium complexes lowers the lipophilicity, which is ascribed to the introduction of the cationic charge, and results in logD<sub>7.4</sub> values in the range 1.49–1.97. The lowest lipophilicity is observed for the complex [Ir(ppy)<sub>2</sub>(MeTzPyCN)]<sup>+</sup> at 0.64. A comparison of the logD<sub>7.4</sub> values between [Ir(ppy)<sub>2</sub>(TzPyCN)], [Ir(ppy)<sub>2</sub>(TzPyPhCN)], [Ir(ppy)<sub>2</sub>(TzQn)], and [Ir(ppy)<sub>2</sub>(TziQn)], shows that extending the conjugation of the tetrazolato ligands increases lipophilicity. A similar trend also holds true for the methylated analogues, [Ir(ppy)<sub>2</sub>(MeTzPyCN)]<sup>+</sup>, [Ir(ppy)<sub>2</sub>(MeTzPyPhCN)]<sup>+</sup>, [Ir(ppy)<sub>2</sub>(MeTzQn)]<sup>+</sup>, and [Ir(ppy)<sub>2</sub>(MeTziQn)]<sup>+</sup>. The introduction of fluoride substituents on aromatic moieties is often associated with an increase in logD<sub>7.4</sub> values.<sup>[68–71]</sup> However, this trend was only observed in the methylated complexes, in which logD<sub>7.4</sub>

increased from 0.64 for [Ir(ppy)<sub>2</sub>(MeTzPyCN)]<sup>+</sup> to 1.86 for [Ir(F<sub>2</sub>ppy)<sub>2</sub>(MeTzPyCN)]<sup>+</sup>. In contrast, little change was observed in the logD<sub>7.4</sub> value between [Ir(ppy)<sub>2</sub>(TzPyCN)] and [Ir(F<sub>2</sub>ppy)<sub>2</sub>(TzPyCN)], consistently with previously published cyclometalated iridium complexes with lipophilicity values around 2.<sup>[24]</sup>

### Cellular uptake and localisation

The cellular uptake for the synthesised iridium complexes was studied by means of ICP-MS measurements, and the results are reported in Table 2. The H9c2 cells were incubated with complexes at 20 μM in cell culture medium (0.2% DMSO) for 30 minutes at 37 °C. The calculated cellular concentration values were obtained assuming an average volume of a single H9c2 cell equal to 2 pL.<sup>[72]</sup> An analysis of the data reveals that the association between internalisation and lipophilicity does not follow a simple trend. For example, three of the neutral complexes, [Ir(F<sub>2</sub>ppy)<sub>2</sub>(TzPyCN)], [Ir(ppy)<sub>2</sub>(TzPyPhCN)], and [Ir(ppy)<sub>2</sub>(TzQn)] exhibit high iridium intracellular concentrations indicating good cellular internalisation. The remaining two complexes, [Ir(ppy)<sub>2</sub>(TzPyCN)] and [Ir(ppy)<sub>2</sub>(TziQn)], exhibit lower intracellular iridium concentrations although their lipophilicity fell within the range of the aforementioned neutral complexes. On the other hand, only the cationic iridium complexes bound to the quinolyl and isoquinolyl tetrazolato ligands exhibit efficient cellular internalisation. The lack of straightforward trends suggests that the mechanism of internalisation might be different for the various complexes.

The cellular localisation of the iridium complexes was investigated via confocal microscopy. Following the same incubation protocol described for the ICP-MS measurements, complexes could be detected in cells by single-photon excitation at 403 nm and were also shown to be compatible with two-photon imaging modalities, with optimal excitation in the range of 810–830 nm (see the Supporting Information). All the complexes could be readily detected within cells in an emission interval of 525–644 nm, (consistent with emissions recorded in the cuvette), allow for co-staining with commercially available organelle markers. The [Ir(ppy)<sub>2</sub>(MeTzPyCN)]<sup>+</sup> complex was not detected in cells, therefore co-localisation studies were not performed for this species.

All the neutral complexes had similar staining patterns and evidenced a diffuse network emanating from the nucleus and extending into the cytoplasm (Figure 6), consistent with the endoplasmic reticulum (ER). In addition, the methylated cationic complex [Ir(ppy)<sub>2</sub>(MeTzQn)]<sup>+</sup> also detected this reticular network in the perinuclear region (Figure 6). Co-staining with ER-Tracker™ revealed relatively high Pearson's correlation coefficients,<sup>[73]</sup> with values above 0.7, confirming these complexes localise within the ER (see the Supporting Information).

Although the neutral complexes and the methylated cationic complex [Ir(ppy)<sub>2</sub>(MeTzQn)]<sup>+</sup> were predominately localised within the ER, their emission was also detected within compartments in the cytoplasm that were not labelled with ER-Tracker™. The morphology and localisation of these compartments resembled lipid droplets. BODIPY® 500/510 C<sub>1</sub>C<sub>12</sub>, a fatty

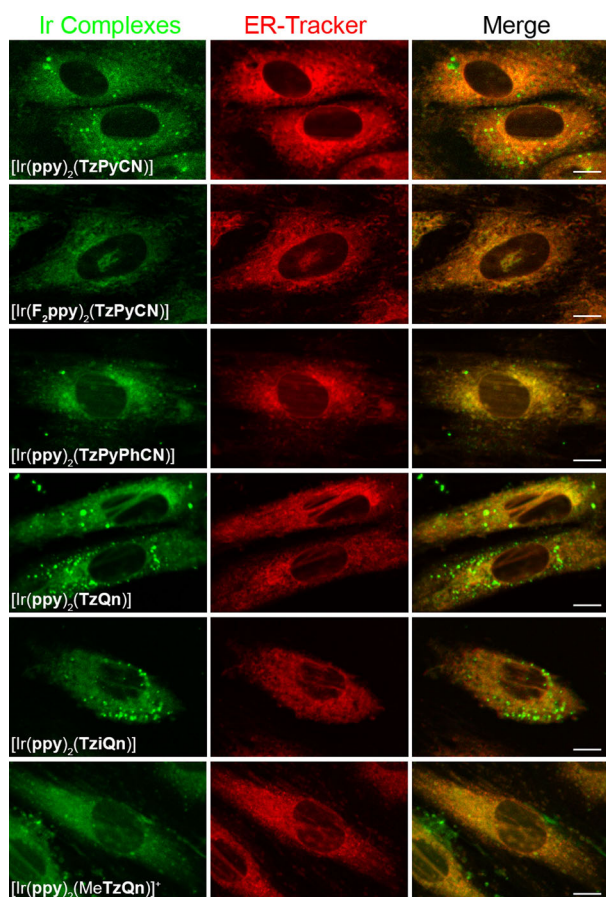


**Figure 6.** Iridium complexes interacting with endoplasmic reticulum (ER) in live H9c2 cells. Micrographs of H9c2 cells stained with the iridium complexes (green) and counter-stained with ER Tracker™ (red). Yellow/orange colour in the merge indicates marker co-localisation. The iridium complexes were excited at 403 nm and the emission was collected in the region 525–644 nm; ER-Tracker was excited at 561 nm and the emission was collected in the region 570–620 nm. Scale bars: 10  $\mu$ m.

acid analogue that localises with lipid droplets and partially with the endoplasmic reticulum, produced strong co-localisation with these complexes (Figure 7). A high Pearson's correlation coefficients was obtained for these complexes and BODIPY® 500/510 C<sub>1</sub>,C<sub>12</sub> (ranging between 0.63 and 0.92; see the Supporting Information),<sup>[73]</sup> confirming that these compartments were lipid droplets.

The methylated complexes  $[\text{Ir}(\text{F}_2\text{ppy})_2(\text{MeTzPyCN})]^+$  and  $[\text{Ir}(\text{ppy})_2(\text{MeTzPyPhCN})]^+$  localised to elongated structures throughout the cytoplasm, a staining pattern that is characteristic of mitochondrial association (Figure 8). Co-staining with MitoTracker® Red CMXRos confirmed this interaction, with Pearson's correlation coefficient between 0.65 and 0.71 (see the Supporting Information).<sup>[73]</sup> It is possible that the positive charge favours the transport of these complexes across the mitochondrial membrane as a consequence of the intermembrane electrical potential gradient. This explanation is consistent with the typical mitochondrial affinity of delocalised lipophilic cations such as phosphonium salts, or previously reported cationic metal complexes.<sup>[74]</sup> It is interesting to note that the complex  $[\text{Ir}(\text{F}_2\text{ppy})_2(\text{MeTzPyCN})]^+$  also stained what

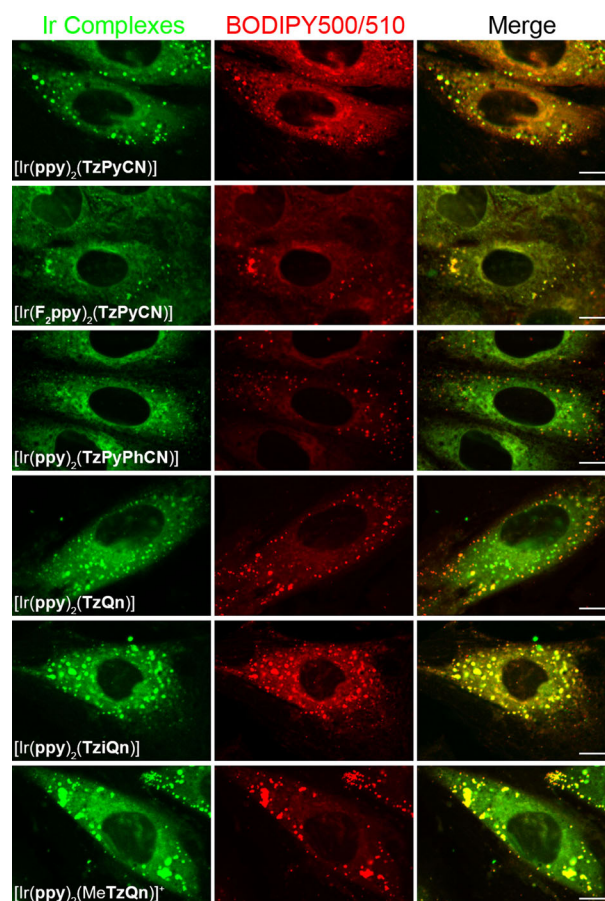


**Figure 7.** Iridium complexes localise with lipid droplets in live H9c2 cells. Micrographs of H9c2 cells stained with the iridium complexes (green) and counter-stained with BODIPY® 500/510 C<sub>1</sub>,C<sub>12</sub> fatty acid analogue (red). Yellow/orange colour in the merge indicates marker co-localisation. The iridium complexes were excited at 403 nm and the emission was collected in the region 525–644 nm; BODIPY500/510 was excited at 488 nm and the emission was collected in the region 500–550 nm. Scale bars: 10  $\mu$ m.

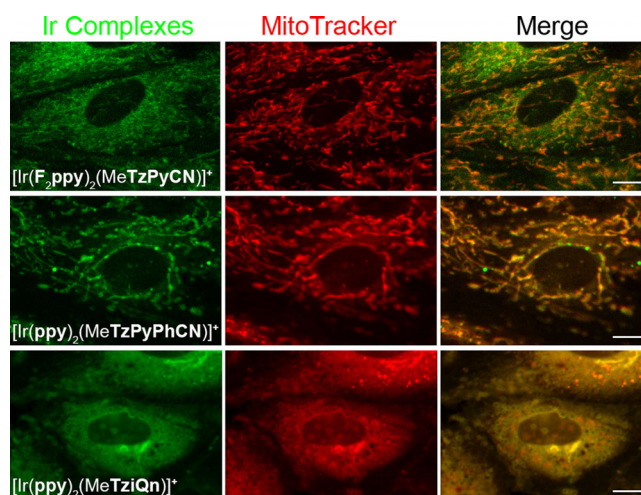


**Figure 8.** Iridium complexes interacting with mitochondria in live H9c2 cells. Micrographs of H9c2 cells stained with the iridium complexes (green) and counter-stained with Mito-Tracker® Red CMXRos (red). Yellow/orange colour in the merge indicates co-localisation between markers. The iridium complexes were excited at 403 nm and the emission was collected in the region 525–644 nm; MitoTracker was excited at 561 nm and the emission was collected in the region 570–620 nm. Scale bars: 10  $\mu$ m.

appears to be the ER along with the mitochondria, although co-staining between the complex and ER-Tracker could not be performed (see the Supporting Information). However,  $[\text{Ir}(\text{ppy})_2(\text{MeTzIQn})]^+$  also co-located with MitoTracker® Red CMXRos, this charged complex appeared to induce apoptosis, characterised by the formation of cellular vacuoles and rounding of the mitochondria (Figure 8). In this case, ER-Tracker™ was also observed to co-localise with these unusual cellular structures. An increase of caspase activity in H9c2 cells after incubation with  $[\text{Ir}(\text{ppy})_2(\text{MeTzIQn})]^+$  confirmed the induction of apoptosis (see the Supporting Information).<sup>[75]</sup>

Confocal microscopy was also employed to assess the mechanism of cellular internalisation. The intensity of the emission from the iridium complexes was compared between cells incubated at 37 and 4 °C (Figure 9), the latter to suppress energy-mediated mechanisms of entrance. The emission detected from each complex shows a good correlation with the average amount of iridium found in cells measured by ICP-MS (Table 2). Cells incubated with  $[\text{Ir}(\text{F}_2\text{ppy})_2(\text{TzPyCN})]$ ,  $[\text{Ir}(\text{ppy})_2(\text{TzPyPhCN})]$ ,  $[\text{Ir}(\text{ppy})_2(\text{TzQn})]$ ,  $[\text{Ir}(\text{ppy})_2(\text{MeTzQn})]^+$  and  $[\text{Ir}(\text{ppy})_2(\text{MeTzIQn})]^+$  show the highest emission intensity, and also record the largest concentration of iridium per cell. The trend in emission intensity also correlates well with the quantum yield values (Table 1). For example, the emission detected from  $[\text{Ir}(\text{ppy})_2(\text{TzPyPhCN})]$  is comparable with  $[\text{Ir}(\text{ppy})_2(\text{MeTzQn})]^+$  and  $[\text{Ir}(\text{ppy})_2(\text{MeTzIQn})]^+$ , even though the former was detected at a lower concentration. The emission detected from each of the cells following incubation at 4 °C was significantly reduced.

This suggests that energy dependent pathways are predominantly involved in the cellular uptake of these complexes, a result that is consistent with previously studied cyclometalated iridium complexes incubated in various cell lines.<sup>[17,26,42,46,76]</sup> Again, the lack of clear trends in Figure 9 suggests variable mechanism of entrance even for subtle chemical changes. For example,  $[\text{Ir}(\text{ppy})_2(\text{TzQn})]$  is detected well upon incubation at 4 °C, but  $[\text{Ir}(\text{ppy})_2(\text{TziQn})]$  is barely visible, even though the two complexes differ only by the orientation of the quinoyl substituents and have very similar lipophilicity values. Our results reinforce previously reported views<sup>[48,77]</sup> that conclusions based exclusively on lipophilicity measurements might not be adequate, even for families of complexes with very similar chemical structures.

### Cytotoxicity

The cell viability was assessed via MTS assay to highlight cytotoxic effects after internalisation of the iridium complexes (without photoexcitation). The H9c2 cells were incubated for either 2 or 24 hours with the complexes at 20 μM or 40 μM. An important trend emerges from the collected results (Figure 10), highlighting the fact that although the neutral complexes only exhibit slight cytotoxicity, cell viability is reduced upon incubation with the corresponding cationic complexes. On comparing the cytotoxicity and ICP-MS data from incubated cells, it is clear that cytotoxic effects are not exclusively dependent on the relative amount of iridium complexes incubated within the

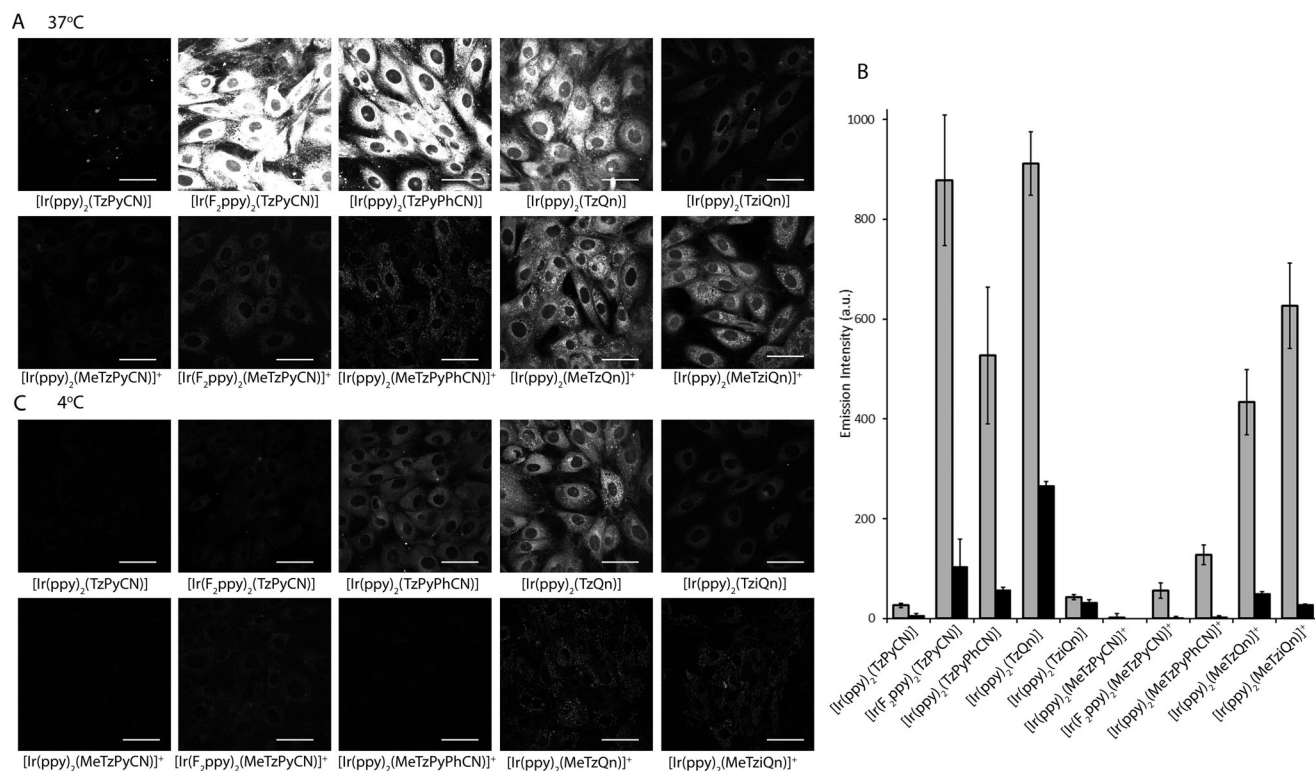


**Figure 9.** Confocal micrographs of H9c2 cells incubated with iridium complexes at 37 °C (A) or 4 °C (C). Scale bars: 50 μm. (B) Histogram showing the emission intensity of iridium complexes detected from H9c2 cells when incubated at 37 °C (grey bars) or 4 °C (black bars) to inhibit energy dependent cell entry.

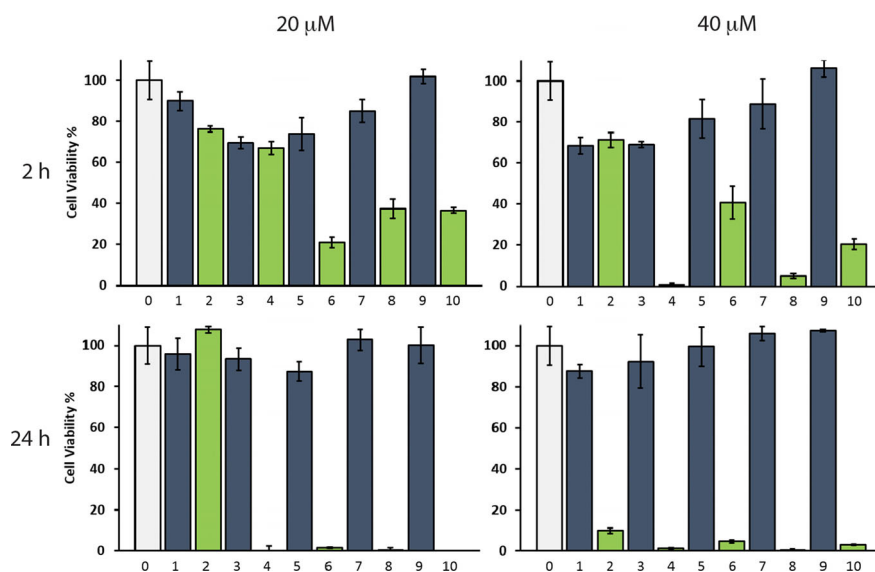


**Figure 10.** Cell viability after 2 and 24 hours incubation with the iridium complexes at 20 and 40  $\mu\text{M}$ . Neutral complexes are represented by blue bars, whereas cationic complexes are represented by green bars. 0) Control (0.2% DMSO in serum-free DMEM media); 1)  $[\text{Ir}(\text{ppy})_2(\text{TzPyCN})]$ ; 2)  $[\text{Ir}(\text{ppy})_2(\text{MeTzPyCN})]^+$ ; 3)  $[\text{Ir}(\text{F}_2\text{ppy})_2(\text{TzPyCN})]$ ; 4)  $[\text{Ir}(\text{F}_2\text{ppy})_2(\text{MeTzPyCN})]^+$ ; 5)  $[\text{Ir}(\text{ppy})_2(\text{TzPyPhCN})]$ ; 6)  $[\text{Ir}(\text{ppy})_2(\text{MeTzPyPhCN})]^+$ ; 7)  $[\text{Ir}(\text{ppy})_2(\text{TzQn})]$ ; 8)  $[\text{Ir}(\text{ppy})_2(\text{MeTzQn})]^+$ ; 9)  $[\text{Ir}(\text{ppy})_2(\text{TziQn})]$ ; and 10)  $[\text{Ir}(\text{ppy})_2(\text{MeTziQn})]^+$ .

cells. For example, the fluorinated complex  $[\text{Ir}(\text{F}_2\text{ppy})_2(\text{TzPyCN})]$  does not exhibit significant cytotoxicity compared to its methylated analogue  $[\text{Ir}(\text{F}_2\text{ppy})_2(\text{MeTzPyCN})]^+$ , even though the concentration of the latter is lower by an order of magnitude. These results suggest that cytotoxic effect for this family of iridium complexes might be strongly related to their relative cellular localisation.

The only exception to the cytotoxic effect of the cationic complexes seems to be related to  $[\text{Ir}(\text{ppy})_2(\text{MeTzPyCN})]^+$ , which from the ICP-MS results showed minimal accumulation within the cells. Unfortunately however, the localisation of this compound could not be assessed due to its non-emissive nature in aqueous medium.

It is well-known that phosphorescent metal complexes act as sensitizers for singlet oxygen.<sup>[78]</sup> Therefore, during imaging with confocal microscopy a resting time of at least 30 seconds is always provided to the cells to recover from a potential increase in reactive oxygen species. This is a protocol we optimised during our previous studies using rhenium complexes as cellular labels.<sup>[79]</sup> Using this protocol, and imaging cells incubated for 30 minutes with a 20  $\mu\text{M}$  solution of iridium complex, blebbing of the cell membrane was never observed. On the other hand, cells incubated under the same conditions and continuously illuminated showed signs of blebbing within a 30 minute timeframe (see the Supporting Information). These results demonstrate that the neutral series of iridium tetrazolato complexes possess very promising properties for the development of iridium-based markers for imaging of the ER in live cells. This is in contrast to other cationic iridium complexes that were previously shown to accumulate in the endoplasmic reticulum, but which were cytotoxic due to the triggering of  $\text{Ca}^{2+}$  release into the cytoplasm.<sup>[80]</sup>

### Photostability

Photobleaching experiments were carried out on H9c2 cells incubated with the iridium complexes at 20  $\mu\text{M}$  for 30 minutes (see SI). The cells were illuminated continuously at 403 nm for 900 s, and the decrease in emission intensity was compared with that from cells incubated with ER-Tracker. All the complexes evaluated in cells showed better photostability than ER-Tracker, with the cationic complexes exhibiting emission intensity above 85% of the initial values after 900 s irradiation. The neutral iridium complexes proved to be slightly more prone to photobleaching, but still displayed emission above 70% of the initial emission intensity after 900 s irradiation. The only exception was the fluorinated  $[\text{Ir}(\text{F}_2\text{ppy})_2(\text{TzPyCN})]$ , which showed a photobleaching profile just slightly slower than ER-Tracker. The data clearly highlight how the cationic complexes exhibit better photostability than their neutral analogues. The same general trend was also observed from photobleaching experiments in cuvettes using  $10^{-5}\text{M}$  aqueous solutions (0.2% DMSO), excited using a Pen-Ray Mercury Lamp source at 365 nm (see the Supporting Information for experimental details).

### Conclusions

This work reports the synthesis of iridium tetrazolato complexes and their potential use as probes in live cells. A library of neutral complexes displaying chemical variations at the cyclometalating phenylpyridine and tetrazolato ligands was synthesised. Furthermore, methylation of these species allowed facile access to the corresponding cationic complexes, so that a SAR for cellular internalisation, localisation, and cytotoxicity could be more systematically investigated. The

photophysical properties of these species revealed typical phosphorescent emission from excited states of charge transfer nature, as a mixture of <sup>3</sup>MLCT and <sup>3</sup>LLCT. The emission of the complexes was found to be in general solvatochromic, with a red-shift occurring upon increase of medium polarity. Quantification of cellular incubation via ICP-MS revealed great variability, with trends that cannot be simply correlated to the degree of lipophilicity and charge of the complexes. These results suggest potentially different mechanisms of uptake, and a comparison of the emission intensity from cells incubated at 37 and 4 °C reveals these are predominantly energy mediated. The majority of the complexes were internalised into cells and detection was possible via either one-photon or two-photon imaging modalities. The neutral species were predominantly localised within the endoplasmic reticulum and to various extents within lipid droplets. On the other hand, the cationic species exhibited more specificity for mitochondria. A marked difference between the neutral and cationic probes was found in terms of cytotoxicity, which was restricted mainly to the charged complexes during long term experiments. The higher cytotoxicity of the cationic complexes does not seem to be exclusively linked to the amount of complex internalised within the cells, and it is potentially highly dependent also on the localisation. This study has therefore highlighted that neutral iridium tetrazolato complexes are suitable building blocks for the design of markers for cellular imaging on long timescales, and more specifically for the imaging of ER and lipid droplets. However, specific protocols for imaging modalities (e.g., resting time between consecutive excitation regimes) are essential to avoid photocytotoxicity. On the other hand, cationic iridium tetrazolato complexes are good candidates for the design of mitochondrial markers. However, careful considerations must be taken for longer time experiments, as these cationic complexes have demonstrated higher cytotoxicity with the respect to their neutral analogues.

## Experimental Section

### General Considerations

Unless otherwise stated, all reagents and solvents were purchased from Sigma Aldrich or Alfa Aesar and used as received without further purification. The species HTzQn,<sup>[81]</sup> HTziQn,<sup>[81]</sup> [Ir(ppy)<sub>2</sub>(μ-Cl)]<sub>2</sub>,<sup>[82]</sup> [Ir(F<sub>2</sub>ppy)<sub>2</sub>(μ-Cl)]<sub>2</sub>,<sup>[82]</sup> and [Ir(ppy)<sub>2</sub>(TzPyBr)]<sup>[11]</sup> were prepared according to previously published procedures. Detailed synthetic procedures for the iridium complexes and corresponding ligands described in this work are reported in the Supporting Information. Nuclear magnetic resonance spectra were recorded using a Bruker Avance 400 spectrometer (400 MHz for <sup>1</sup>H NMR; 100 MHz for <sup>13</sup>C NMR) at 300 K. All NMR spectra were calibrated to residual solvent signals. Infrared spectra were recorded using an attenuated total reflectance PerkinElmer Spectrum 100 FT-IR with a diamond stage. IR spectra were recorded from 4000–650 cm<sup>-1</sup>. The intensity of the band is reported as strong (s), medium (m), or weak (w), with broad (br) bands also specified. Melting points were determined using a BI Barnsted Electrothermal 9100 apparatus. Elemental analyses were carried out on bulk samples using a Thermo Finning EA 1112 Series Flash; the presence of solvents in the bulk samples was further confirmed by <sup>1</sup>H NMR.

### X-ray crystallography

Crystallographic data for the structure were collected at 100(2) K on an Oxford Diffraction Gemini diffractometer with Mo Kα or Cu Kα radiation. Following absorption corrections and solution by direct methods, the structures were refined against F<sup>2</sup> with full-matrix least-squares using the program SHELXL-2014.<sup>[83]</sup> All hydrogen atoms were added at calculated positions and refined by use of riding models with isotropic displacement parameters based on those of the parent atoms. Anisotropic displacement parameters were employed throughout for the non-hydrogen atoms. Structure refinement data are reported in the Supporting Information.

CCDC 1506221 ([Ir(F<sub>2</sub>ppy)<sub>2</sub>(TzPyCN)]) and 1506222 ([Ir(ppy)<sub>2</sub>(MeTzPyMeCN)][PF<sub>6</sub>]) contain the supplementary crystallographic data for this paper. These data are provided free of charge by The Cambridge Crystallographic Data Centre.

### Photophysical measurements

Absorption spectra were recorded at room temperature using a Cary 4000 UV/Vis spectrometer. Uncorrected steady state emission and excitation spectra were recorded on an Edinburgh FLSP980-S2S2-stm spectrometer equipped with: i) a temperature-monitored cuvette holder; ii) 450 W Xenon arc lamp; iii) double excitation and emission monochromators; iv) a Peltier cooled Hamamatsu R928P photomultiplier tube (spectral range 200–870 nm). Emission and excitation spectra were corrected for source intensity (lamp and grating) and emission spectral response (detector and grating) by a calibration curve supplied with the instrument. According to the approach described by Demas and Crosby,<sup>[84]</sup> luminescence quantum yields (Φ<sub>em</sub>) were measured in optically dilute solutions (O.D. < 0.1 at excitation wavelength) obtained from absorption spectra on a wavelength scale [nm] and compared to the reference emitter by Equation (1):

$$\Phi_x = \Phi_r \left[ \frac{A_r(\lambda_r)}{A_x(\lambda_x)} \right] \left[ \frac{I_r(\lambda_r)}{I_x(\lambda_x)} \right] \left[ \frac{n_x^2}{n_r^2} \right] \left[ \frac{D_x}{A_r} \right]$$

where *A* is the absorbance at the excitation wavelength (*λ*), *I* is the intensity of the excitation light at the excitation wavelength (*λ*), *n* is the refractive index of the solvent, *D* is the integrated intensity of the luminescence and Φ is the quantum yield. The subscripts *r* and *x* refer to the reference and the sample, respectively. The quantum yield determinations were performed at identical excitation wavelength for the sample and the reference, therefore cancelling the *I*(*λ*<sub>r</sub>)/*I*(*λ*<sub>x</sub>) term in the equation. The quantum yields of complexes were measured against an aqueous solution of [Ru(bipy)<sub>3</sub>]Cl<sub>2</sub> (bipy = 2,2'-bipyridine; Φ<sub>r</sub> = 0.028).<sup>[85]</sup> Emission lifetimes (τ) were determined with the time-correlated single-photon counting technique (TCSPC) with the same Edinburgh FLSP980-S2S2-stm spectrometer using either a pulsed picosecond LED (EPLD/EPL 377 nm, FWHM < 800 ps). The goodness of fit was assessed by minimising the reduced χ<sup>2</sup> function and by visual inspection of the weighted residuals. The solvents used for the preparation of the solutions for the photophysical investigations were of LR grade and the water was deionised. Degassing of the dichloromethane solutions was performed using the freeze-pump-thaw method. Experimental uncertainties are estimated to be ± 8% for lifetime determinations, ± 20% for quantum yields, ± 2 nm and ± 5 nm for absorption and emission peaks, respectively.

## TD-DFT

Time-dependent density functional theory calculations were performed with GAUSSIAN 09.<sup>[86]</sup> Prior to these calculations, the structures were relaxed at the B3LYP level of theory.<sup>[87,88]</sup> The Ir atoms were treated with the Stuttgart-Dresden effective core potential,<sup>[89]</sup> the Pople 6-311G\*\* basis set was used for all the other atoms, and the effect of the solvent was mimicked with the PCM solvation model,<sup>[90]</sup> with parameters adequate for dichloromethane. The low-lying singlet-singlet excitation energies were calculated at the same level of theory, and the spectra were reproduced as the superposition of Gaussian functions with heights proportional to calculated intensities and a variance of 11 nm.

## Cell culture

H9c2 rat cardiomyoblast cells were maintained in high-glucose (4500 mg L<sup>-1</sup>) DMEM medium (Sigma-Aldrich, USA) containing 10% fetal bovine serum (FBS; In Vitro Technologies, USA) and 2 mM L-glutamine (Sigma-Aldrich, USA) at 37 °C and 5% CO<sub>2</sub>. The H9c2 cells were cultured in 75 mm<sup>2</sup> flasks. Cells that had been passaged for no more than 18 times, were used for experiments. For ICP-MS, H9c2 cells were seeded at 2.7 × 10<sup>4</sup> cells mL<sup>-1</sup> and grown in T25 flasks for 72 h, when 100% confluence was reached. For live cell imaging and MTS assay, the H9c2 cells were seeded at 1 × 10<sup>5</sup> cells mL<sup>-1</sup> and cultured overnight in either ibidi  $\mu$ -slide 8 wells in a final volume of 250  $\mu$ L or 96-well microtiter plate in a final volume of 200  $\mu$ L.

## ICP-MS

The H9c2 cells were incubated with the iridium complexes at 20  $\mu$ M (prepared in DMEM full culture media with 0.2% DMSO) for 30 minutes at 37 °C and 5% CO<sub>2</sub>. The cells were washed three times with phosphate buffered saline (PBS), and then detached with TripLE Express reagent (Gibco, USA) for 2 minutes. The cells were then washed from T25 flasks with 3 mL of DMEM full culture medium, and pelleted by centrifugation at 400 rpm for 10 minutes. The medium was removed and the cells were resuspended in 2 mL of PBS for cells counts. The remaining cells were centrifuged at 1000 rpm for 10 minutes, the medium was then removed leaving behind the stained cell pellets, which were desiccated for 3.5 h at 95 °C. The pellets were reconstituted in 36% HCl (400  $\mu$ L) and left at 95 °C until dry in order to digest organic material. The dry samples were then reconstituted in 2% HCl (2.5 mL) and sonicated for 10 minutes before filtering (pore diameter of 0.2  $\mu$ m). The total iridium determination was performed with an Agilent 8900x triple quad ICP-MS (Agilent Technologies, USA), using He gas (4 mL min<sup>-1</sup>).

## Cell staining

H9c2 cells were incubated with the iridium complexes at 20  $\mu$ M in DMEM full culture medium with 0.2% DMSO for 30 minutes at either 37 °C or 4 °C. The cells were washed twice with PBS, before imaging in DMEM. For co-staining experiments, the cells were then incubated with ER-Tracker™ Red, MitoTracker® Red CMXRos, or BODIPY® 500/510 C<sub>1</sub>,C<sub>12</sub> (Life Technologies Australia Pty Ltd, Australia), following manufacturer's instructions.

## Confocal microscopy

Single-photon live cell imaging was performed using a Nikon A1+ confocal microscope (Nikon, Japan) with a OKOLab Microscope Incubator (Okolab USA Inc., USA). The iridium complexes were excit-

ed at 403 nm and the emission was collected in the 525–644 nm region; ER-Tracker and MitoTracker were excited at 561 nm and the emission was collected in the region 570–620 nm. BODIPY 500/510 was excited at 488 nm and the emission was collected in the region 500–550 nm. Image analysis including, co-localisation and emission intensity was measured using NIS elements V4.50 software (Nikon, Japan). The final preparation of the images was conducted with Adobe Photoshop CC (Adobe Systems Inc., USA). Two-photon microscopy imaging was performed using a Zeiss LSM710 META NLO inverted microscope supplemented with a two-photon Mai-Tai®, tunable Ti:Sapphire femtosecond pulse laser (710–920 nm, Spectra-Physics). The emission from the iridium complexes was detected using the following settings: two-photon excitation wavelength at 830 nm, beam splitter MBS 690+, emission interval 520–650 nm. The images were acquired using a Plan-APO-CHROMAT 63X/ NA1.4 oil immersion objective. The final preparation of the images was conducted with Adobe Photoshop CC (Adobe Systems Inc., USA).

## MTS cell viability assay

The cellular NADPH-dependent redox activity was measured using CellTiter 96® Aqueous Non-Radioactive Cell Proliferation Assay (MTS), according to the manufacturer's instruction (Promega, USA). The H9c2 cells were stained with the iridium complexes at either 20  $\mu$ M or 40  $\mu$ M in DMEM full cell culture medium with 0.2% DMSO, and held at 37 °C and 5% CO<sub>2</sub> for 4 or 24 hours. As a control, H9c2 cells were incubated for the same length of time in DMEM with 0.2% DMSO. Following addition of MTS, the cells incubation for a further 2 hours at 37 °C and 5% CO<sub>2</sub>. The absorbance of the formazan dye was measured by EnVision multi-label plate reader (PerkinElmer, Beaconsfield, UK) at 490 nm. The data are reported as the mean  $\pm$  SEM of three biological replicates for each group.

## Supporting Information

The Supporting Information contains: synthetic details; <sup>1</sup>H and <sup>13</sup>C spectra; X-ray refinement data; all the photophysical details in the various solvent systems including absorption, excitation, and emission spectra, excited state lifetime decays; TD-DFT calculation for [Ir(ppy)<sub>2</sub>(TzQn)] and [Ir(ppy)<sub>2</sub>(TziQn)], confocal imaging via two-photon excitation of live H9c2 cells; Pearson's co-localisation coefficient table; caspase assay for cells incubated with [Ir(ppy)(MeTziQn)]<sup>+</sup>; live cell response to imaging conditions; photostability of the iridium complexes in cells and cuvette.

## Acknowledgements

M.M. and P.R. wishes to thank the ARC for funding (FT130100033 and FT130100463). D.A.B. and J.L.M. wishes to thank the NHMRC for funding (APP1092904 and APP1066916, respectively). C.C. wishes to thank Curtin University for the IPRA scholarship. The authors acknowledge the facilities, and the scientific and technical assistance of the Australian Microscopy & Microanalysis Research Facility at the Centre for Microscopy, Characterisation & Analysis, at the University of Western Australia, a facility funded by the University, State and Commonwealth Governments. The authors acknowledge Adelaide Microscopy, University of Adelaide, South Australia. This research was undertaken with the assistance of resources from

the National Computational Infrastructure (NCI), which is supported by the Australian Government.

**Keywords:** imaging agents · iridium · luminescence · tetrazoles

- [1] M. P. Coogan, V. Fernández-Moreira, *Chem. Commun.* **2014**, *50*, 384–399.
- [2] K. K.-W. Lo in *Topics in Organometallic Chemistry, Vol 29: Photophysics of Organometallics* (Ed.: A. J. Lees), Springer-Verlag, Heidelberg, **2010**, pp. 115–158.
- [3] L. E. Wedlock, S. J. Berners-Price, *Aust. J. Chem.* **2011**, *64*, 692–704.
- [4] M. Mauro, A. Aliprandi, D. Septiadi, N. S. Kehr, L. De Cola, *Chem. Soc. Rev.* **2014**, *43*, 4144–4166.
- [5] D. Parker, *Aust. J. Chem.* **2011**, *64*, 239–243.
- [6] E. New, A. Congreve, D. Parker, *Chem. Sci.* **2010**, *1*, 111–118.
- [7] K. K.-W. Lo, *Acc. Chem. Res.* **2015**, *48*, 2985–2995.
- [8] S. W. Botchway, M. Charnley, J. W. Haycock, A. W. Parker, D. L. Rochester, J. A. Weinstein, J. A. G. Williams, *Proc. Natl. Acad. Sci. USA* **2008**, *105*, 16071–16076.
- [9] K. K.-W. Lo, S. P.-Y. Li, *RSC Adv.* **2014**, *4*, 10560–10585.
- [10] K. K.-W. Lo, D. Ng, C. Chung, *Organometallics* **2001**, *20*, 4999–5001.
- [11] S. Stagni, S. Colella, A. Palazzi, G. Valenti, S. Zacchini, F. Paolucci, M. Marcaccio, R. Q. Albuquerque, L. De Cola, *Inorg. Chem.* **2008**, *47*, 10509–10521.
- [12] L. Flamigni, A. Barbieri, C. Sabatini, B. Ventura, F. Barigelletti, *Top. Curr. Chem.* **2007**, *281*, 143–203.
- [13] Q. Zhao, M. Yu, L. Shi, S. Liu, C. Li, M. Shi, Z. Zhou, C. Huang, F. Li, *Organometallics* **2010**, *29*, 1085–1091.
- [14] S. P.-Y. Li, T. S.-M. Tang, K. S.-M. Yiu, K. K.-W. Lo, *Chem. Eur. J.* **2012**, *18*, 13342–13354.
- [15] L. Murphy, A. Congreve, L.-O. Pålsson, J. A. G. Williams, *Chem. Commun.* **2010**, *46*, 8743–8745.
- [16] M. Yu, Q. Zhao, L. Shi, F. Li, Z. Zhou, H. Yang, T. Yi, C. Huang, *Chem. Commun.* **2008**, *0*, 2115–2117.
- [17] B. Wang, Y. Liang, H. Dong, T. Tan, B. Zhan, J. Cheng, K. K.-W. Lo, Y.-W. Lam, S.-H. Cheng, *ChemBioChem* **2012**, *13*, 2729–2737.
- [18] W. H.-T. Law, L. C.-C. Lee, M.-W. Louie, H.-W. Liu, T. W.-H. Ang, K. K.-W. Lo, *Inorg. Chem.* **2013**, *52*, 13029–13041.
- [19] K. K.-W. Lo, B. T.-N. Chan, H.-W. Liu, K. Y. Zhang, S. P.-Y. Li, T. S.-M. Tang, *Chem. Commun.* **2013**, *49*, 4271–4273.
- [20] K. Y. Zhang, H.-W. Liu, M.-C. Tang, A. W.-T. Choi, N. Zhu, X.-G. Wei, K.-C. Lau, K. K.-W. Lo, *Inorg. Chem.* **2015**, *54*, 6582–6593.
- [21] L. Sun, Y. Chen, S. Kuang, G. Li, R. Guan, J. Liu, L. Ji, H. Chao, *Chem. Eur. J.* **2016**, *22*, 8955–8965.
- [22] K. K.-S. Tso, K.-K. Leung, H.-W. Liu, K. K.-W. Lo, *Chem. Commun.* **2016**, *52*, 4557–4560.
- [23] P. Steunenbergh, A. Ruggi, N. S. van den Berg, T. Buckle, J. Kuil, F. W. B. van Leeuwen, A. H. Velders, *Inorg. Chem.* **2012**, *51*, 2105–2114.
- [24] L. He, Y. Li, C.-P. Tan, R.-R. Ye, M.-H. Chen, J.-J. Cao, L.-N. Ji, Z.-W. Mao, *Chem. Sci.* **2015**, *6*, 5409–5418.
- [25] K. Qiu, H. Huang, B. Liu, Y. Liu, Z. Huang, Y. Chen, L. Ji, H. Chao, *ACS Appl. Mater. Interfaces* **2016**, *8*, 12702–12710.
- [26] K. Y. Zhang, S. P.-Y. Li, N. Zhu, I. W.-S. Or, M. S.-H. Cheung, Y.-W. Lam, K. K.-W. Lo, *Inorg. Chem.* **2010**, *49*, 2530–2540.
- [27] C. Li, M. Yu, Y. Sun, Y. Wu, C. Huang, F. Li, *J. Am. Chem. Soc.* **2011**, *133*, 11231–11239.
- [28] A. Wragg, M. R. Gill, D. Turton, H. Adams, T. M. Roseveare, C. Smythe, X. Su, J. A. Thomas, *Chem. Eur. J.* **2014**, *20*, 14004–14011.
- [29] A. Wragg, M. R. Gill, L. McKenzie, C. Glover, R. Mowll, J. A. Weinstein, X. Su, C. Smythe, J. A. Thomas, *Chem. Eur. J.* **2015**, *21*, 11865–11871.
- [30] S. Stimpson, D. R. Jenkinson, A. Sadler, M. Latham, D. A. Wragg, A. J. H. M. Meijer, J. A. Thomas, *Angew. Chem. Int. Ed.* **2015**, *54*, 3000–3003; *Angew. Chem.* **2015**, *127*, 3043–3046.
- [31] J. S.-Y. Lau, P.-K. Lee, K. H.-K. Tsang, C. H.-C. Ng, Y.-W. Lam, S.-H. Cheng, K. K.-W. Lo, *Inorg. Chem.* **2009**, *48*, 708–718.
- [32] S.-K. Leung, H.-W. Liu, K. K.-W. Lo, *Chem. Commun.* **2011**, *47*, 10548–10550.
- [33] K. K.-W. Lo, S.-K. Leung, C.-Y. Pan, *Inorg. Chim. Acta* **2012**, *380*, 343–349.
- [34] K. Koren, R. I. Dmitriev, S. M. Borisov, D. B. Papkovsky, I. Klimant, *ChemBioChem* **2012**, *13*, 1184–1190.
- [35] K. K.-W. Lo, W. H.-T. Law, J. C.-Y. Chan, H.-W. Liu, K. Y. Zhang, *Metalomics* **2013**, *5*, 808–812.
- [36] S.-K. Leung, K. Y. Kwok, K. Y. Zhang, K. K.-W. Lo, *Inorg. Chem.* **2010**, *49*, 4984–4995.
- [37] K. K.-W. Lo, J. S.-Y. Lau, *Inorg. Chem.* **2007**, *46*, 700–709.
- [38] A. Baschieri, S. Muzzioli, V. Fiorini, E. Matteucci, M. Massi, L. Sambri, S. Stagni, *Organometallics* **2014**, *33*, 6154–6164.
- [39] K. K.-W. Lo, J. S.-W. Chan, L.-H. Lui, C.-K. Chung, *Organometallics* **2004**, *23*, 3108–3116.
- [40] T. U. Connell, J. L. James, A. R. White, P. S. Donnelly, *Chem. Eur. J.* **2015**, *21*, 14146–14155.
- [41] L. C.-C. Lee, J. C.-W. Lau, H.-W. Liu, K. K.-W. Lo, *Angew. Chem. Int. Ed.* **2015**, *54*, 11097–11101; *Angew. Chem.* **2015**, *127*, 11249–11253.
- [42] C. Li, Y. Liu, Y. Wu, Y. Sun, F. Li, *Biomaterials* **2013**, *34*, 1223–1234.
- [43] Y. Tang, H.-R. Yang, H.-B. Sun, S.-J. Liu, J.-X. Wang, Q. Zhao, X.-M. Liu, W.-J. Xu, S.-B. Li, W. Huang, *Chem. Eur. J.* **2013**, *19*, 1311–1319.
- [44] Y. Ma, H. Liang, Y. Zeng, H. Yang, C.-L. Ho, W. Xu, Q. Zhao, W. Huang, W.-Y. Wong, *Chem. Sci.* **2016**, *7*, 3338–3346.
- [45] K. J. Castor, K. L. Metera, U. M. Tefashe, C. J. Serpell, J. Mauzeroll, H. F. Sleiman, *Inorg. Chem.* **2015**, *54*, 6958–6967.
- [46] Y. You, S. Cho, W. Nam, *Inorg. Chem.* **2014**, *53*, 1804–1815.
- [47] Y. Wu, H. Jing, Z. Dong, Q. Zhao, H. Wu, F. Li, *Inorg. Chem.* **2011**, *50*, 7412–7420.
- [48] Q. Zhao, C. Huang, F. Li, *Chem. Soc. Rev.* **2011**, *40*, 2508–2524.
- [49] L. He, C.-P. Tan, R.-R. Ye, Y.-Z. Zhao, Y.-H. Liu, Q. Zhao, L.-N. Ji, Z.-W. Mao, *Angew. Chem. Int. Ed.* **2014**, *53*, 12137–12141; *Angew. Chem.* **2014**, *126*, 12333–12337.
- [50] G. Gupta, A. Das, N. B. Ghate, T. Kim, J. Y. Ryu, J. Lee, N. Mandal, C. Y. Lee, *Chem. Commun.* **2016**, *52*, 4274–4277.
- [51] Z. Liu, L. Salassa, A. Habtemariam, A. M. Pizarro, *Inorg. Chem.* **2011**, *50*, 5777–5783.
- [52] W. Tan, J. Zhou, F. Li, T. Yi, H. Tian, *Chem. Asian J.* **2011**, *6*, 1263–1268.
- [53] Y. Zhou, J. Jia, W. Li, H. Fei, M. Zhou, *Chem. Commun.* **2013**, *49*, 3230–3232.
- [54] C. A. Bader, R. D. Brooks, Y. S. Ng, A. Sorvina, M. V. Werrett, P. J. Wright, A. G. Anwer, D. A. Brooks, S. Stagni, S. Muzzioli, *RSC Adv.* **2014**, *4*, 16345–16351.
- [55] C. A. Bader, T. Shandala, E. A. Carter, A. Ivask, T. Guinan, S. M. Hickey, M. V. Werrett, P. J. Wright, P. V. Simpson, S. Stagni, *PLoS ONE* **2016**, *11*, e0161557.
- [56] C. A. Bader, E. A. Carter, A. Safitri, P. V. Simpson, P. Wright, S. Stagni, M. Massi, P. A. Lay, D. A. Brooks, S. E. Plush, *Mol. BioSyst.* **2016**, *12*, 2064–2068.
- [57] C. A. Bader, A. Sorvina, P. V. Simpson, P. J. Wright, S. Stagni, S. E. Plush, M. Massi, D. A. Brooks, *FEBS Lett.* **2016**, *590*, 3051–3060.
- [58] M. V. Werrett, G. S. Huff, S. Muzzioli, V. Fiorini, S. Zacchini, B. W. Skelton, A. Maggiore, J. M. Malicka, M. Cocchi, K. C. Gordon, *Dalton Trans.* **2015**, *44*, 8379–8393.
- [59] M. V. Werrett, S. Muzzioli, P. J. Wright, A. Palazzi, P. Raiteri, S. Zacchini, M. Massi, S. Stagni, *Inorg. Chem.* **2014**, *53*, 229–243.
- [60] Z. P. Demko, K. B. Sharpless, *Org. Lett.* **2002**, *4*, 2525–2527.
- [61] Z. P. Demko, K. B. Sharpless, *J. Org. Chem.* **2001**, *66*, 7945–7950.
- [62] V. Balzani, G. Bergamini, S. Campagna, F. Puntoriero, *Top. Curr. Chem.* **2007**, *280*, 1–36.
- [63] V. Fiorini, A. D'Ignazio, K. D. M. MaGee, M. I. Ogden, M. Massi, S. Stagni, *Dalton Trans.* **2016**, *45*, 3256–3259.
- [64] C. D. Ertl, L. Gil-Escrig, J. Cerdá, A. Pertegás, H. J. Bolink, J. M. Junquera-Hernández, A. Prescimone, M. Neuburger, E. C. Constable, E. Orti, *Dalton Trans.* **2016**, *45*, 11668–11681.
- [65] P.-T. Chou, Y. Chi, M.-W. Chung, C.-C. Lin, *Coord. Chem. Rev.* **2011**, *255*, 2653–2665.
- [66] Y. W. I. Low, F. Blasco, P. Vachaspati, *Eur. J. Pharm. Sci.* **2016**, *92*, 110–116.
- [67] A. M. Courtis, S. A. Santos, Y. Guan, J. A. Hendricks, B. Ghosh, D. M. Szantai-Kis, S. A. Reis, J. V. Shah, R. Mazitschek, *Bioconjugate Chem.* **2014**, *25*, 1043–1051.
- [68] S. Purser, P. R. Moore, S. Swallow, V. Gouverneur, *Chem. Soc. Rev.* **2008**, *37*, 320–330.

- [69] F.-X. Wang, M.-H. Chen, X.-Y. Hu, R.-R. Ye, C.-P. Tan, L.-N. Ji, Z.-W. Mao, *Sci. Rep.* **2016**, *6*, 38958.
- [70] J.-J. Cao, C.-P. Tan, M.-H. Chen, N. Wu, D.-Y. Yao, X.-G. Liu, L.-N. Ji, Z.-W. Mao, *Chem. Sci.* **2017**, *8*, 631–640.
- [71] J. Liu, C. Jin, B. Yuan, X. Liu, Y. Chen, L. Ji, H. Chao, *Chem. Commun.* **2017**, *53*, 2052–2055.
- [72] K. E. Merten, Y. Jiang, W. Feng, Y. J. Kang, *J. Pharm. Exp. Therap.* **2006**, *319*, 934–940.
- [73] J. Adler, I. Parmryd, *Cytometry* **2010**, *77A*, 733–742.
- [74] J. S. Modica-Napolitano, J. R. Aprille, *Adv. Drug Delivery Rev.* **2001**, *49*, 63–70.
- [75] S. H. Kaufmann, S.-H. Lee, X. W. Meng, D. A. Loegering, T. J. Kottke, A. J. Henzing, S. Ruchaud, K. Samejima, W. C. Earnshaw, *Methods* **2008**, *44*, 262–272.
- [76] K. K.-W. Lo, K. Y. Zhang, *RSC Adv.* **2012**, *2*, 12069–12083.
- [77] V. Fernández-Moreira, F. L. Thorp-Greenwood, M. P. Coogan, *Chem. Commun.* **2010**, *46*, 186–202.
- [78] P. Ogilby, *Chem. Soc. Rev.* **2010**, *39*, 3181–3209.
- [79] M. V. Werrett, P. J. Wright, P. V. Simpson, P. Raiteri, B. W. Skelton, S. Stagni, A. G. Buckley, P. J. Rigby, M. Massi, *Dalton Trans.* **2015**, *44*, 20636–20647.
- [80] R. Cao, J. Jia, X. Ma, M. Zhou, H. Fei, *J. Med. Chem.* **2013**, *56*, 3636–3644.
- [81] V. Fiorini, A. M. Ranieri, S. Muzzioli, K. D. M. MaGee, S. Zacchini, N. Akabar, A. Stefan, M. I. Ogden, M. Massi, S. Stagni, *Dalton Trans.* **2015**, *44*, 20597–20608.
- [82] S. Sprouse, K. A. King, P. J. Spellane, R. J. Watts, *J. Am. Chem. Soc.* **1984**, *106*, 6647–6653.
- [83] G. M. Sheldrick, *Acta Crystallogr. Sect. A* **2008**, *64*, 112–122.
- [84] G. A. Crosby, J. N. Demas, *J. Phys. Chem.* **1971**, *75*, 991–1024.
- [85] K. Nakamaru, *Bull. Chem. Soc. Jpn.* **1982**, *55*, 2697–2705.
- [86] Gaussian 09, Revision B.01, M. J. Frisch, G. W. Trucks, H. B. Schlegel, G. E. Scuseria, M. A. Robb, J. R. Cheeseman, G. Scalmani, V. Barone, B. Men- nucci, G. A. Petersson, H. Nakatsuji, M. Caricato, X. Li, H. P. Hratchian, A. F. Izmaylov, J. Bloino, G. Zheng, J. L. Sonnenberg, M. Hada, M. Ehara, K. Toyota, R. Fukuda, J. Hasegawa, M. Ishida, T. Nakajima, Y. Honda, O. Kitao, H. Nakai, T. Vreven, J. A. Montgomery, Jr., J. E. Peralta, F. Ogliaro, M. Bearpark, J. J. Heyd, E. Brothers, K. N. Kudin, V. N. Staroverov, R. Kobayashi, J. Normand, K. Raghavachari, A. Rendell, J. C. Burant, S. S. Iyengar, J. Tomasi, M. Cossi, N. Rega, J. M. Millam, M. Klene, J. E. Knox, J. B. Cross, V. Bakken, C. Adamo, J. Jaramillo, R. Gomperts, R. E. Stratmann, O. Yazyev, A. J. Austin, R. Cammi, C. Pomelli, J. W. Ochterski, R. L. Martin, K. Morokuma, V. G. Zakrzewski, G. A. Voth, P. Salvador, J. J. Dannenberg, S. Dapprich, A. D. Daniels, Ö. Farkas, J. B. Foresman, J. V. Ortiz, J. Cio- slowski, D. J. Fox, Gaussian, Inc. Wallingford CT, **2009**.
- [87] C. Lee, W. Yang, R. Parr, *Phys. Rev. B* **1988**, *37*, 785–789.
- [88] A. D. Becke, *J. Chem. Phys.* **1993**, *98*, 1372–1377.
- [89] D. Andrae, U. Haeussermann, M. Dolg, H. Stoll, H. Preuss, *Theor. Chim. Acta* **1990**, *77*, 123–141.
- [90] J. Tomasi, B. Mennucci, R. Cammi, *Chem. Rev.* **2005**, *105*, 2999–3094.

---

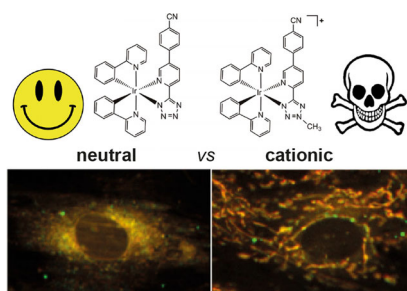
Manuscript received: March 24, 2017

Accepted manuscript online: ■ ■ ■ ■, 0000

Version of record online: ■ ■ ■ ■, 0000

## FULL PAPER

**A glowing family in cell:** Neutral iridium tetrazolato complexes provide exceptional building block for the design of molecular probes for the endoplasmic reticulum in live cells, while methylation causes the complexes to shift interaction to the mitochondria and exhibit enhanced cytotoxicity.



## Fluorescent Probes

*C. Caporale, C. A. Bader, A. Sorvina, K. D. M. MaGee, B. W. Skelton, T. A. Gillam, P. J. Wright, P. Raiteri, S. Stagni, J. L. Morrison, S. E. Plush,\* D. A. Brooks,\* M. Massi\**



**Investigating Intracellular Localisation and Cytotoxicity Trends for Neutral and Cationic Iridium Tetrazolato Complexes in Live Cells**

